

## Trigonal warping effect of carbon nanotubes

R. Saito

*Department of Electronic-Engineering, University of Electro-Communications, Chofu, Tokyo 182-8585, Japan*

G. Dresselhaus

*Francis Bitter Magnet Laboratory, Massachusetts Institute of Technology, Cambridge, Massachusetts 02139*

M. S. Dresselhaus

*Department of Physics and Department of Electrical Engineering and Computer Science,  
Massachusetts Institute of Technology, Cambridge, Massachusetts 02139*

(Received 27 September 1999)

Chirality-dependent van Hove singularities (vHs) of the one-dimensional electronic density of states (DOS) are discussed in connection with resonant Raman spectroscopy. The effect of trigonal warping on the energy dispersion relations near the Fermi energy splits the peaks of the density of states for metallic nanotubes, and the magnitude of this effect depends on the chiral angle of the carbon nanotube. The width of the peak splitting has a maximum for metallic zigzag nanotubes, and no splitting is obtained for armchair nanotubes or semi-conducting nanotubes. We also find an additional logarithmic singularity in the electronic DOS for carbon nanotubes that is related to a two-dimensional singularity, which does not depend on either the diameter or the chirality.

### I. INTRODUCTION

One-dimensional van Hove singularities (vHs) in the electronic density of states (DOS), which are known to be proportional to  $(E^2 - E_0^2)^{-1/2}$  at both the energy minima and maxima ( $\pm E_0$ ) of the dispersion relations for carbon nanotubes, are important for determining many solid state properties of carbon nanotubes, such as the spectra observed by scanning tunneling spectroscopy (STS),<sup>1-4</sup> optical absorption,<sup>5-7</sup> and resonant Raman spectroscopy.<sup>8-11</sup> The energy positions  $E_0$  of the vHs peaks have been discussed within the linear  $k$  approximation of the energy bands of carbon nanotubes as these energy bands relate to two-dimensional (2D) graphite in the vicinity of the Fermi energy.<sup>12,13</sup> Within the linear  $k$  approximation for the energy dispersion relations of graphite, the energy positions of the vHs do not depend on the chirality but only on the diameter of the nanotube. Here we show that, when the linear  $k$  approximation is relaxed and the dispersion relations are treated in more detail, the energy of the vHs peaks *also depend on the chirality* of the carbon nanotubes.

Recently, Kataura and coworkers plotted the energy differences between the  $i$ th vHs peaks in the conduction and valence bands numbered from the Fermi energy,  $E_{ii}(d_i)$ , as a function of nanotube diameter  $d_i$  for all chiral angles at a given  $d_i$  value, and his calculation of the energy differences  $E_{ii}(d_i)$  was based on the tight-binding approximation for the energy bands.<sup>6</sup> Kataura showed that the energy differences between the vHs peaks  $E_{ii}(d_i)$  have a width in energy for fixed  $d_i$  and that this width increases with increasing energy relative to the Fermi energy.<sup>6,14</sup> Kataura and co-workers also showed that the width of the peak positions of the vHs at constant  $d_i$  was consistent with the experimental width of the peaks in the optical absorption spectra for single-wall nanotube (SWNT) rope samples and with the experimental reso-

nant Raman spectra for the same sample.<sup>6,14</sup> However, the physical origin of the width of the peak positions is not clear from their papers.

In this paper, we investigate the Kataura plot in detail, and we find that the peak positions of the vHs do indeed depend on the nanotube chirality and that the origin of the width of the peak positions can be explained by the so-called trigonal warping effect of the energy bands, whereby equi-energy contours in the Brillouin zone of graphite change from circles around the  $K$  points for the linear  $k$  regime to a triangular shape around the  $M$  points (see Fig. 1). This theoretical result is important in the sense that STS and resonant Raman spectroscopy experiments<sup>8,10,11</sup> depend on the chirality of an individual SWNT, and therefore trigonal warping effects should provide experimental information about the chiral angle of carbon nanotubes. Although the chiral angle is directly observed by scanning tunneling microscopy (STM),<sup>15</sup>

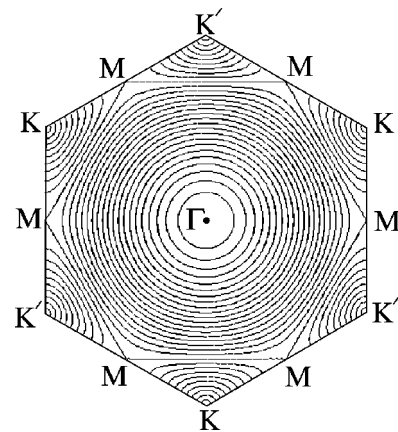


FIG. 1. The contour plot of 2D energy of graphite. The equi-energy contours are circles near  $K$  and near the center of the Brillouin zone, but near the zone boundary the contours are straight lines which connect nearest  $M$  points.

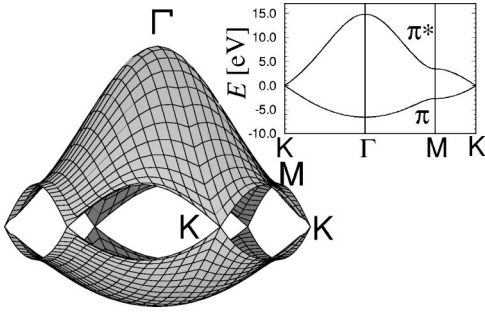


FIG. 2. The energy dispersion relations for the  $\pi$  and  $\pi^*$  bands in 2D graphite are shown throughout the whole region of the Brillouin zone. The inset shows the energy dispersion along the high symmetry directions of the 2D Brillouin zone.

corrections to the experimental observation are necessary to account for the effect of the tip shape and of the deformation of the nanotube on the substrate.<sup>16</sup> We expect that the chirality-dependent DOS spectra are insensitive to such effects.

Concerning the application of the zone-folding method to the graphite  $\pi$  energy bands in which only the nearest-neighbor carbon-carbon interaction energy,  $\gamma_0$ , is included, three possible effects are considered in connection with first-principles calculations of the electronic structure of carbon nanotubes: (1) the effect of curvature on  $\gamma_0$ , (2) the inclusion of the tight binding overlap integral  $s$ , which is associated with the asymmetry between the valence and conduction bands in 2D graphite,<sup>17</sup> and (3) the trigonal warping effect in which the equi-energy contours change from a circle to a triangular shape with increasing energy.

The curvature effect has been discussed within the Slater-Koster method in which the correction to the  $\gamma_0$  of a SWNT with the diameter  $d_t$  is given by<sup>18,19</sup>

$$\gamma_0(d_t) = \gamma_0(\infty) \left\{ 1 - \frac{1}{2} \left( \frac{a_{C-C}}{d_t} \right)^2 \right\}. \quad (1)$$

Here,  $a_{C-C}$  is the nearest-neighbor carbon-carbon distance, which is taken to be 1.44 Å for a SWNT. The factor 1/2 in Eq. (1) comes from averaging over the direction of the chemical bonds of each carbon atom relative to the nanotube axis. The relative correction to  $\gamma_0(d_t)$  is thus only  $(a_{C-C}/d_t)^2 \sim 10^{-2}$  for  $d_t = 1.4$  nm corresponding to a (10,10) armchair nanotube. Here, the nanotube diameter  $d_t$  is related to the nanotube integers  $(n, m)$  by

$$d_t = \sqrt{3} a_{C-C} (m^2 + mn + n^2)^{1/2} / \pi. \quad (2)$$

Thus, the curvature effect is generally neglected except for very small diameter nanotubes, since the smallest nanotubes with a  $C_{60}$  fullerene diameter [such as a (5,5) nanotube] would have only about a 2% decrease in the value for  $\gamma_0$  due to nanotube curvature. Lambin<sup>19</sup> showed that this small correction is sufficient to account for the strain energy of 0.08 eV nm<sup>2</sup>/d<sub>t</sub><sup>2</sup> found in carbon nanotubes due to the curvature of the graphene sheet.

A nonzero value for the overlap integral  $s$  modifies the electronic energy at the  $M$  point (edge center of the hexagonal Brillouin zone, see Fig. 2), from  $\pm \gamma_0$  to  $\pm \gamma_0 / (1 \mp s)$  for the  $\gamma_0 > 0$ . When we use the values of  $\gamma_0 = 2.9$  eV and  $s = 0.129$ , the energy values for the  $\pi^*$  and  $\pi$  bands at the  $M$  point become +3.329 and -2.568 eV. These values for the  $M$  point energies show an asymmetry (see Fig. 2) that is important for considering intraband optical transitions within either the conduction or valence bands for doped carbon nanotubes<sup>7</sup>. However, when we consider the energy difference between the conduction and valence bands, the overlap effect (i.e., nonzero value for  $s$ ) is not so significant for energies less than 3 eV, since the energy difference at the  $M$  point is modified only by a factor  $2\gamma_0 / (1 - s^2)$ , proportional to  $s^2$ . Thus, the effect of a nonzero  $s$  value on the interband energy difference between vHs in the valence and conduction bands is only on the order of  $10^{-2}$ .

Thus, for SWNT's with diameters of around 1~2 nm and for excitation energies below 3 eV, which is the usual situation for observation of the resonant Raman scattering in SWNT's,<sup>8,10,11</sup> the trigonal warping effect becomes the most important of the three effects enumerated above, especially for metallic nanotubes, as is discussed in this paper.

In Sec. II, we give a brief summary on how to calculate the electronic density of states for SWNT's, and in Sec. III, we show the calculated results for the vHs peak positions as a function of the chirality. In Sec. IV, relevant experiments are discussed and in Sec. V, a summary of the results are given.

## II. ASYMMETRY OF THE ELECTRONIC STRUCTURE OF 2D GRAPHENE AND 1D NANOTUBES

The 1D electron density of states are given by the energy dispersion of carbon nanotubes which is obtained by zone folding of the 2D energy dispersion relation of graphite. The 2D energy dispersion relations of graphite are calculated<sup>17</sup> by solving the eigenvalue problem for a  $(2 \times 2)$  Hamiltonian  $\mathcal{H}$  and a  $(2 \times 2)$  overlap integral matrix  $\mathcal{S}$ , associated with the two distinct  $A$ - and  $B$ -atom sites in 2D graphite,

$$\mathcal{H} = \begin{pmatrix} \epsilon_{2p} & -\gamma_0 f(k) \\ -\gamma_0 f(k)^* & \epsilon_{2p} \end{pmatrix} \quad \text{and} \quad \mathcal{S} = \begin{pmatrix} 1 & sf(k) \\ sf(k)^* & 1 \end{pmatrix}, \quad (3)$$

where  $\epsilon_{2p}$  is the site energy of the  $2p$  atomic orbital and

$$f(k) = e^{ik_x a / \sqrt{3}} + 2e^{-ik_x a / 2\sqrt{3}} \cos \frac{k_y a}{2}. \quad (4)$$

Here,  $a = \sqrt{3} a_{C-C}$ . Solution of the secular equation

$$\det(\mathcal{H} - E\mathcal{S}) = 0 \quad (5)$$

implied by Eq. (3) leads to the eigenvalues

$$E_{g2D}^{\pm}(\vec{k}) = \frac{\epsilon_{2p} \pm \gamma_0 w(\vec{k})}{1 \mp s w(\vec{k})} \quad (6)$$

for  $\gamma_0 > 0$ , and  $E^+$  and  $E^-$  correspond to the valence  $\pi$  and the conduction  $\pi^*$  energy bands, respectively. The function  $w(\vec{k})$  in Eq. (6) is given by

$$w(\vec{k}) = \sqrt{|f(\vec{k})|^2} = \sqrt{1 + 4 \cos^2 \frac{\sqrt{3}k_x a}{2} \cos^2 \frac{k_y a}{2} + 4 \cos^2 \frac{k_y a}{2}}. \quad (7)$$

In Fig. 2, we plot the electronic energy dispersion relations for 2D graphite as a function of the two-dimensional  $k$  values in the hexagonal Brillouin zone. The corresponding energy contour plot of the 2D energy bands of graphite with  $s=0$  is shown in Fig. 1.

Near the  $K$  point at the corner of the hexagonal Brillouin zone of graphite,  $w(\vec{k})$  has a linear dependence on  $k \equiv |\vec{k}|$  measured from the  $K$  point as

$$w(\vec{k}) = \frac{\sqrt{3}}{2}ka + \dots, \quad \text{for } ka \ll 1. \quad (8)$$

Thus, the expansion of Eq. (6) for small  $k$  yields

$$E_{g2D}^{\pm}(\vec{k}) = \epsilon_{2p} \pm (\gamma_0 - s\epsilon_{2p})w(\vec{k}) + \dots, \quad (9)$$

so that in this approximation the valence and conduction bands are symmetric near the  $K$  point, independent of the value of  $s$ . When we adopt  $\epsilon_{2p}=0$  and  $s=0$  for Eq. (6), and assume a linear  $k$  approximation for  $w(k)$ , we get the linear dispersion relation for graphite given by<sup>20,21</sup>

$$E(k) = \pm \frac{\sqrt{3}}{2} \gamma_0 ka = \pm \frac{3}{2} \gamma_0 ka_{C-C}. \quad (10)$$

If the physical phenomena under consideration only involve small  $k$  vectors, it is convenient to use Eq. (10) for interpreting experimental results relevant to such phenomena.

The asymmetry in the valence- and conduction-band energy dispersion relations in Eq. (6) arises from the quadratic terms in  $w(\vec{k})$  and this asymmetry becomes important for large  $k$  values. For a 2D graphene sheet, the values of the tight binding parameters  $\epsilon_{2p}=0$ ,  $\gamma_0=3.033$  eV, and  $s=0.129$  fit both the first-principles calculation of the energy bands of turbostratic graphite<sup>18,22</sup> and experimental data.<sup>17,23</sup> The nonzero value of  $s$  leads to an overall asymmetry between the bonding and antibonding states of 2D graphite for large  $k$  as measured with respect to the  $K$  point. This asymmetry effect is shown in Fig. 2, where the symmetry-imposed degeneracy between the valence and conduction bands at the  $K$  point in the Brillouin zone is seen. At the  $M$  and  $\Gamma$  points, which are far from the  $K$  point (see Figs. 1 and 2), the 2D graphite energies calculated from Eq. (6) are  $E_{g2D}^{\pm}(M) = \pm \gamma_0/(1 \mp s)$  and  $E_{g2D}^{\pm}(\Gamma) = \pm 3 \gamma_0/(1 \mp 3s)$  which display the asymmetry between valence- and conduction-band energies described above. We also note that the energy differences  $E_{g2D}^+(M) - E_{g2D}^-(M) = 2 \gamma_0/(1 - s^2)$  and  $E_{g2D}^+(\Gamma) - E_{g2D}^-(\Gamma) = 6 \gamma_0/(1 - 9s^2)$  are not as sensitive to  $s$  for typical values for  $s$ , and these energy differences become larger when  $s \neq 0$ . Thus, if  $s$  is assumed to be nonzero, the  $\gamma_0$  value estimated from measurements relevant to the  $\Gamma$  or  $M$  points in the Brillouin zone should be smaller than the  $\gamma_0$  obtained from analysis of experiments relevant to the  $K$  point. Also, the value obtained for  $\gamma_0$  from fits to experimental data will depend somewhat on the value assigned to  $s$ . Furthermore, if  $s > 0$ , different values can be obtained for  $\gamma_0$  when different physical phenomena are mea-

sured, since different phenomena will in general be sensitive to  $E(\mathbf{k})$  at different  $\mathbf{k}$  values. On the other hand, various physical phenomena can, in principle, be used to determine an experimental value for  $s$ , which would provide a more complete description of the dispersion relations for the nanotubes.

The 1D energy dispersion relations of a single wall carbon nanotube are given by

$$E_{\mu}(k) = E_{g2D} \left( k \frac{\mathbf{K}_2}{|\mathbf{K}_2|} + \mu \mathbf{K}_1 \right), \quad (11)$$

$$\left( \mu = 1, \dots, N, \text{ and } -\frac{\pi}{T} < k < \frac{\pi}{T} \right),$$

where  $T$  is the magnitude of the unit cell vector along the nanotube axis,  $k$  is a wave vector along the nanotube axis and  $N$  is the number of hexagons of the graphite honeycomb lattice that lie within the nanotube unit cell, and  $N$  is given by

$$N = \frac{2(n^2 + m^2 + nm)}{d_R}. \quad (12)$$

Here  $d_R$  is the greatest common divisor of  $(2n+m)$  and  $(2m+n)$  for a  $(n,m)$  nanotube.<sup>17</sup> Further  $\mathbf{K}_1$  and  $\mathbf{K}_2$  denote, respectively, a discrete unit wave vector along the circumferential direction, and a reciprocal lattice vector along the nanotube axis direction, which are given for a  $(n,m)$  nanotube by

$$\mathbf{K}_1 = \{(2n+m)\mathbf{b}_1 + (2m+n)\mathbf{b}_2\}/Nd_R \quad (13)$$

$$\mathbf{K}_2 = (m\mathbf{b}_1 - n\mathbf{b}_2)/N,$$

where  $\mathbf{b}_1$  and  $\mathbf{b}_2$  are the reciprocal lattice vectors of two-dimensional graphite and are given by

$$\mathbf{b}_1 = \left( \frac{1}{\sqrt{3}}, 1 \right) \frac{2\pi}{a}, \quad \mathbf{b}_2 = \left( \frac{1}{\sqrt{3}}, -1 \right) \frac{2\pi}{a}, \quad (14)$$

in  $x,y$  coordinates.

The periodic boundary condition for a carbon nanotube  $(n,m)$  gives  $N$  discrete  $k$  values in the circumferential direction. The direction of the discrete  $k$  vectors and the separation between two adjacent  $k$  vectors are both given by the  $\mathbf{K}_1$  vector shown in Fig. 3. Here we show one  $K$  point and only a few of the  $N$  possible  $\mathbf{K}_1$  vectors. In the direction of the carbon nanotube axis, which is expressed by the  $\mathbf{K}_2$  vector, we can define continuous  $k$  vectors in the one-dimensional Brillouin zone for each  $\mathbf{K}_1$  vector.

The  $N$  pairs of energy dispersion curves given by Eq. (11) correspond to the cross sections of the two-dimensional energy dispersion surface shown in Fig. 2, where cuts are made on the lines of  $k\mathbf{K}_2/|\mathbf{K}_2| + \mu\mathbf{K}_1$ . If for a particular  $(n,m)$  nanotube, the cutting line passes through a  $K$  point of the 2D Brillouin zone (Fig. 2), where the  $\pi$  and  $\pi^*$  energy bands of two-dimensional graphite are degenerate by symmetry, then the one-dimensional energy bands have a zero energy gap.

The 1D density of states (DOS) in units of states/C atom/eV is calculated by

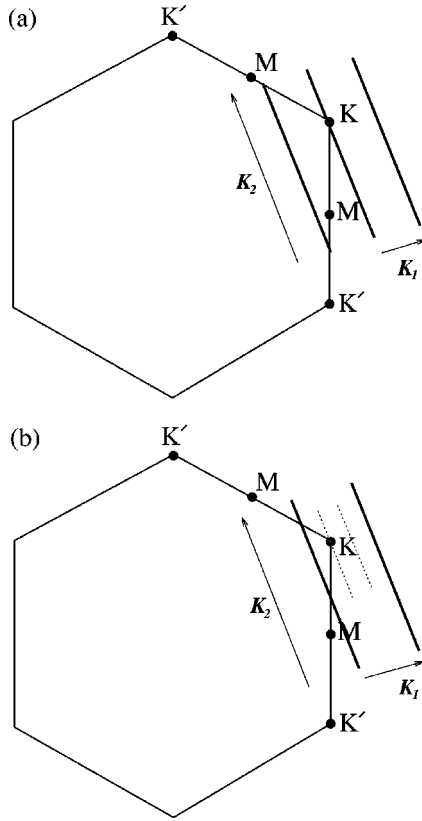


FIG. 3. The wave vector  $k$  for one-dimensional carbon nanotubes is shown in the two-dimensional Brillouin zone of graphite (hexagon) as bold lines for (a) metallic and (b) semiconducting carbon nanotubes. In the direction of  $\mathbf{K}_1$ , discrete  $k$  values are obtained by periodic boundary conditions for the circumferential direction of the carbon nanotubes, while in the direction of the  $\mathbf{K}_2$  vector, continuous  $k$  vectors are shown in the one-dimensional Brillouin zone. (a) For metallic nanotubes, the bold line intersects a  $K$  point (corner of the hexagon) at the Fermi energy of graphite. (b) For the semiconductor nanotubes, the  $K$  point always appears one-third of the distance between two bold lines. It is noted that only a few of all the possible bold lines are shown near the indicated  $K$  point. For each  $\mathbf{K}_1$  vector, there is an energy minimum in the valence and conduction energy subbands, giving rise to the energy differences  $E_{ii}(d_i)$ .

$$D(E) = \frac{2}{N} \sum_{\mu=1}^N \int \frac{1}{\left| \frac{dE_{\mu}(k)}{dk} \right|} \delta(E_{\mu}(k) - E) dE. \quad (15)$$

The integrated value of  $D(E)$  for the energy region of  $E_{\mu}(k)$  is 4, which includes the spin degeneracy for any  $(n, m)$  nanotube and includes the plus and minus signs of  $E_{g2D}$ . It is clear from Eq. (15) that the density of states becomes large when the energy dispersion relation becomes flat as a function of  $k$ .

### III. CALCULATED RESULTS

The peaks in the 1D electronic density of states of the conduction band measured from the Fermi energy, corresponding to the van Hove singularities, are shown in Fig. 4 for several *metallic*  $(n, m)$  nanotubes, all having about the same diameter  $d_i$  (from 1.31 to 1.43 nm), but different chiral

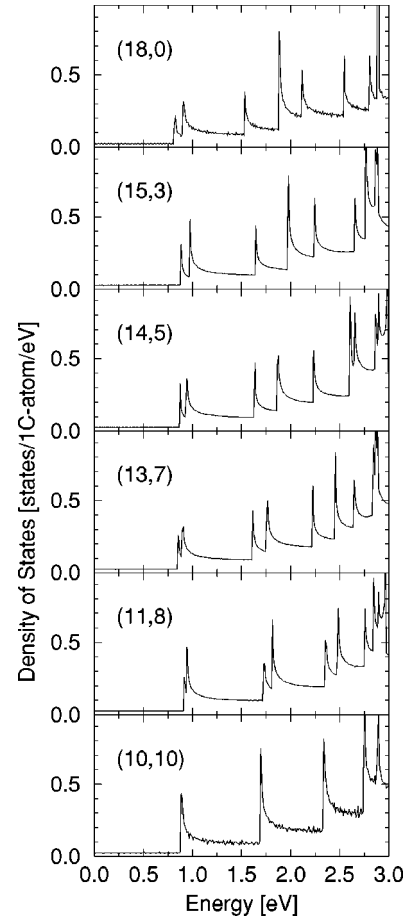


FIG. 4. The 1D electronic density of states vs energy for several metallic nanotubes of approximately the same diameter, showing the effect of chirality on the van Hove singularities: (10,10) (armchair), (11,8), (13,7), (14,5), (15,3), and (18,0) (zigzag).

angles  $\theta = \arctan\{\sqrt{3}m/(2n+m)\}$  between  $0 \leq |\theta| \leq 30^\circ$ , including  $\theta = 0^\circ$  for a zigzag nanotube (18,0),  $\theta = 30^\circ$  for an armchair nanotube (10,10), and 4 nanotubes with chiral angles,  $8.9^\circ$ ,  $14.7^\circ$ ,  $20.2^\circ$ , and  $24.8^\circ$  for the chiral nanotubes (15,3), (14,5), (13,7), and (11,8), respectively. When we look at the peaks in the 1D DOS from the bottom ( $\theta = 30^\circ$ ) to the top ( $\theta = 0^\circ$ ) of Fig. 4, the first DOS peaks around  $E = 0.9$  eV are split into two peaks whose separation in energy (width) increases with decreasing chiral angle, though the average energy position is similar for all these nanotubes which have similar diameters. The width of the splitting of the second peak around  $E = 1.7$  eV is larger than that of the first peak for the same SWNT. In the case of the (14,5) nanotube, the width of the splitting of the second peak is as large as the separation to the split third peaks  $E_{33}(d_i)$ . It is clear from Fig. 4 that the DOS is significantly chirality dependent, and the reason for this effect is discussed below.

The average energy position of the peaks depends on the nanotube diameter, which is explained<sup>12,13</sup> by the linear dispersion approximation of Eq. (10). The energy difference  $E_{11}(d_i)$  between the highest-lying valence-band singularity and the lowest-lying conduction-band singularity in the 1D density of states for the electronic 1D density of states curves for metallic and semiconducting nanotubes shows that  $E_{11}^M(d_i)$  is three times as large for the metallic nanotubes for

which  $n - m = 3q$ , where  $q$  is an integer, as for the semiconducting tubes  $E_{11}^S(d_t)$ , for which  $n - m \neq 3q$ . Using Eq. (10), we can write simple analytic expressions for metallic [ $E_{11}^M(d_t)$ ] and semiconducting [ $E_{11}^S(d_t)$ ] nanotubes as follows:

$$E_{11}^M(d_t) = 6a_{C-C}\gamma_0/d_t \quad (16)$$

and

$$E_{11}^S(d_t) = 2a_{C-C}\gamma_0/d_t. \quad (17)$$

Equations (16) and (17) are derived as follows. In Fig. 3, we show the allowed wave vectors  $k$  as bold lines and we show the reciprocal lattice wave vectors  $\mathbf{K}_1$  and  $\mathbf{K}_2$  for a one-dimensional carbon nanotube in the hexagonal Brillouin zone of two-dimensional graphite for (a) metallic and (b) semiconducting carbon nanotubes. The one-dimensional van Hove singularities of carbon nanotubes near the Fermi energy come from the energy dispersions along the bold lines in Fig. 3 near the  $K$  point of the Brillouin zone of 2D graphite. For the metallic carbon nanotubes, one bold line in Fig. 3 goes right through a  $K$  point, and this intersection gives rise to the zero energy band gap at the  $K$  point (see Fig. 2), while for the semiconducting nanotubes, the  $K$  point is always located in a position one third of the distance between two adjacent  $\mathbf{K}_1$  lines.<sup>24</sup> The energy minimum of each subband near the  $K$  point corresponds to a peak that is a van Hove singularity.

Using the linear approximation for the energy dispersion relation  $E(k)$  of Eq. (10), the energy differences between the van Hove singularities are expressed by substituting for  $k$  the values of  $\mathbf{K}_1$  for metallic nanotubes and of  $\mathbf{K}_1/3$  and  $2\mathbf{K}_1/3$  for semiconducting nanotubes, respectively. After a simple calculation using Eq. (13) for  $\mathbf{K}_1$  for carbon nanotubes, we get the important relation

$$|\mathbf{K}_1| = 2/d_t. \quad (18)$$

Substituting the value of  $|\mathbf{K}_1| = 2/d_t$  into Eq. (10), we get the formulas for  $E_{11}$  given by Eqs. (16) and (17). For isolated single-wall nanotubes, use of the linear  $k$  approximation in Eq. (10), allows us to write the relation  $E_{11}^M(d_t) = 3E_{11}^S(d_t)$  at the same value of  $d_t$ .<sup>12</sup> With these approximations for a semiconducting nanotube of given  $d_t$ , resonant energy differences occur at  $E_{11}^S(d_t)$ ,  $2E_{11}^S(d_t)$ ,  $4E_{11}^S(d_t)$ ,  $5E_{11}^S(d_t)$ ,  $7E_{11}^S(d_t)$ , ... and for metallic nanotubes, resonant energy differences occur at  $E_{11}^M(d_t)$ ,  $2E_{11}^M(d_t)$ , ...

When the value of  $|\mathbf{K}_1| = 2/d_t$  is large, which corresponds to smaller values of  $d_t$ , the linear dispersion approximation is no longer correct. When we then plot equi-energy lines near the  $K$  point (see Fig. 1), we get circular contours for small  $k$  values near the  $K$  and  $K'$  points in the Brillouin zone, but for large  $k$  values, the equi-energy contour becomes a triangle, which connects the three  $M$  points nearest to the  $K$  point (see Fig. 5). The distortion of the equi-energy lines away from the circular contour in materials with a threefold symmetry axis is known as the trigonal warping effect. Thus the energy minima positions on the bold lines shown in Fig. 3 are not always at the closest positions to the  $K$  point. Therefore, the energy minima positions now depend on the

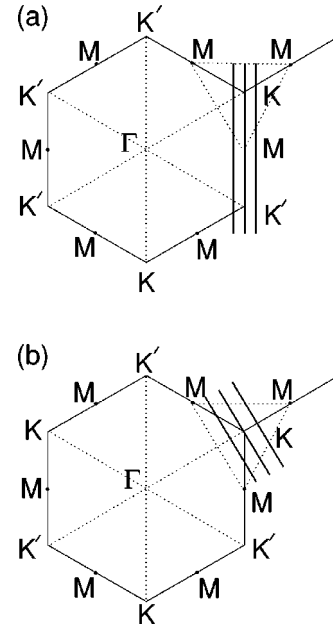


FIG. 5. The dependence of the trigonal warping effect of the van Hove singularities on the nanotube chirality. The three bold lines near the  $K$  point are possible  $k$  vectors in the hexagonal Brillouin zone of graphite for metallic (a) armchair and (b) zigzag carbon nanotubes. All chiral nanotubes with chiral angles  $|\theta| \leq \pi/6$  have lines for their  $k$  vectors with the directions making a chiral angle  $\theta$  measured from the bold lines for the zigzag nanotubes. The minimum energy along the neighboring two lines gives the energy positions of the van Hove singularities.

direction of the  $\mathbf{K}_2$  vectors, as is also shown in Fig. 3, from which we conclude that the energy minima positions depend on the chirality of the carbon nanotubes.

Trigonal warping effects generally split the singular peaks in the 1D density of states for metallic nanotubes, which come from the two nearest possible  $\mathbf{K}_1$  vectors near the  $K$  point (see Fig. 5). Although there are  $N$  inequivalent lines which give  $2N$  energy subbands for  $(n, m)$  carbon nanotubes, only the line that goes through the  $K$  point and neighboring lines are shown for simplicity in Fig. 3. The minimum energies along the neighboring two lines give the energy positions of the van Hove singularities. Although the distances of the two lines from the  $K$  points are the same, the two lines are in general inequivalent in the 2D reciprocal lattice and thus the two lines have a different energy minimum with respect to each other. This is the physical reason why the DOS peaks are split.

On the other hand, for semiconducting nanotubes, we consider the minima for the energy subbands by changing the distance of the allowed  $k$  vector lines to  $1/3$  of that between the two lines near the  $K$  point in Fig. 3. Since the value of the  $k$  vectors on the two lines near the  $K$  point contribute to different spectra, namely that of  $E_{11}^S(d_t)$  and  $E_{22}^S(d_t)$ , there is no splitting of the DOS for semiconducting nanotubes. It is pointed out here that there are two equivalent  $K$  points in the hexagonal Brillouin zone denoted by  $K$  and  $K'$  as shown in Fig. 3, and the values of  $E_{ii}^S(d_t)$  are the same for the  $K$  and  $K'$  points. This is because the  $K$  and  $K'$  points are related to one another by time reversal symmetry (they are at opposite corners from each other in the hexagonal

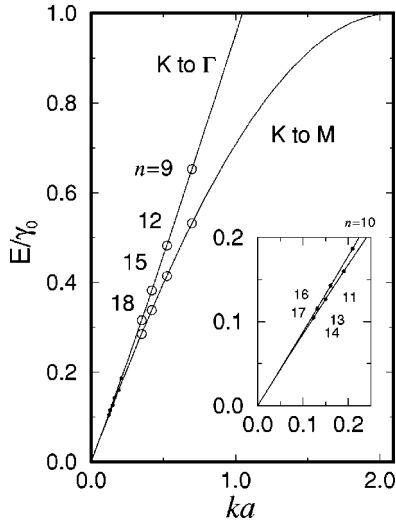


FIG. 6. Trigonal warping effect for zigzag nanotubes. Two energy minimum positions in the conduction band for zigzag nanotubes,  $(n,0)$  measured from the energy at the  $K$  point. Open circles denote metallic carbon nanotubes for  $k=|\mathbf{K}_1|$  vectors away from the  $K$  point along the  $K \rightarrow M$  and  $K \rightarrow \Gamma$  lines, which is the direction of the energy minima (see Fig. 5). The closed circles denote semiconducting carbon nanotubes for  $k=|\mathbf{K}_1|/3$  vectors. (The inset shows an expanded view of the figure at small  $E/\gamma_0$  and small  $ka$  for semiconducting nanotubes.) Note that the maximum of the horizontal axis corresponds to the  $M$  point,  $ka=2\pi/3$ , which is measured from the  $K$  point. A nanotube diameter of 1 nm corresponds to a (13,0) carbon nanotube.

Brillouin zone), and because the chirality is invariant under the time-reversal operation. Thus, the DOS for semiconducting nanotubes will be split if very strong magnetic fields are applied in the direction of nanotube axis.

When we compare Figs. 1 and 5(a), the energy minimum position of an armchair nanotube, which is always metallic, is shifted from the closest point to the  $K$  point to the lines connecting  $K$  and the upper two  $M$  points. Further, when we compare Figs. 1 and 5(b), the energy minimum positions of a metallic zigzag nanotube denoted by  $(3n,0)$  is on the line connecting the  $K$  point to the  $\Gamma$  point in the hexagonal Brillouin zone and on the line connecting the  $K$  point to the  $M$  point going in the opposite direction from  $K$  to  $\Gamma$ . Since the energy dispersions on the  $K-\Gamma$  and  $K-M$  lines are different from each other, the energy minimum values are different, though the distance from the  $K$  point to the energy minimum points are equal (see Fig. 1). This is the reason why we get a splitting of the DOS peaks for general metallic nanotubes. Only armchair nanotubes do not show such a splitting, and the splitting becomes a maximum for metallic zigzag nanotubes. In general, the splitting increases monotonically with decreasing chiral angle and diameter, as shown in Fig. 4 for the dependence on chiral angle, and in Fig. 6, which is discussed below, for the dependence on nanotube diameter.

In Fig. 6 the energies of the van Hove singularities corresponding to the lowest 1D energy level are plotted for metallic (open circles) and semiconducting (closed circles) zigzag nanotubes  $(n,0)$  along the directions  $K \rightarrow M$  and along  $K \rightarrow \Gamma$  for nanotubes of different diameters. The splitting of  $E_{ii}^M$  is a maximum for zigzag nanotubes, which determines the width of the DOS peaks for rope samples. Using Eqs. (7)

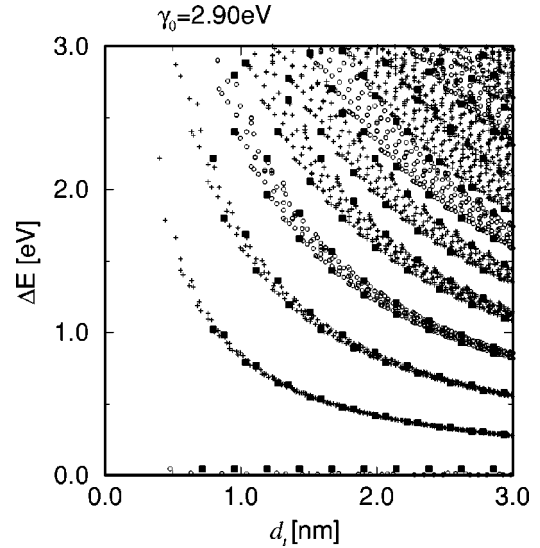


FIG. 7. Calculation of the energy separations  $E_{ii}(d_t)$  for all  $(n,m)$  values as a function of nanotube diameter between  $0.7 < d_t < 3.0$  nm [based on the work of Kataura *et al.* (Ref. 6)]. The results are based on the tight binding model of Eqs. (6) and (7), with  $\gamma_0 = 2.9$  eV and  $s=0$ . The crosses and open circles denote the peaks of semiconducting and metallic nanotubes, respectively. Filled squares denote the  $E_{ii}(d_t)$  values for zigzag nanotubes which determine the width of each  $E_{ii}(d_t)$  curve. Note the points for zero gap metallic nanotubes along the abscissa.

and (18), the widths of  $E_{11}^M$  and  $E_{11}^S$ , denoted by  $\Delta E_{11}^M$  and  $\Delta E_{11}^S$ , respectively, are determined by the zigzag nanotubes, and are analytically given by

$$\Delta E_{11}^M(d_t) = 8\gamma_0 \sin^2\left(\frac{a}{2d_t}\right) \quad (19)$$

$$\Delta E_{11}^S(d_t) = 8\gamma_0 \sin^2\left(\frac{a}{6d_t}\right).$$

Although this trigonal warping effect is proportional to  $(a/d_t)^2$ , the terms in Eq. (19) are not negligible, since this correction is the leading term in the expressions for the width  $\Delta E_{ii}(d_t)$  and the factor 8 before  $\gamma_0$  makes this correction meaningful for  $d_t = 1.4$  nm. In fact,  $E_{11}(d_t)$  is split by about 0.18 eV for the (18,0) zigzag nanotube, and this splitting should be observable by STS experiments. Although the trigonal warping effect is larger for metallic nanotubes than for semiconducting nanotubes of comparable diameters, the energy difference of the third peaks  $E_{33}^S(d_t) = 8\gamma_0 \sin^2(2a/3d_t)$  between the (17,0) and (19,0) zigzag nanotubes is about 0.63 eV, using an average  $d_t$  value of 1.43 nm, which becomes easily observable in the experiments. These calculations show that the trigonal warping effect is important for metallic single-wall zigzag nanotubes with diameters  $d_t < 2$  nm. The direct measurement of the chirality by the STM technique and the measurement of the splitting of the DOS by STS on the *same* nanotube would provide very important confirmation of this prediction.

In Fig. 7, we plot all  $E_{ii}$  values as a function of nanotube diameter for all possible chiralities  $(n,m)$  with diameters between  $0.7 \leq d_t \leq 3.0$  nm. The results are based on the tight

binding model of Eqs. (6) and (7), with  $\gamma_0=2.9$  eV and  $s=0$ . The crosses and open circles denote the vHs peaks of semiconducting and metallic nanotubes, respectively. The width of the  $E_{ii}(d_t)$  band at constant  $d_t$  is due to the trigonal warping effect. In fact in Fig. 7, the specific  $E_{ii}(d_t)$  for the zigzag nanotubes,  $(n,0)$ , denoted by the filled squares, are due to the trigonal warping effect shown in Fig. 6. For metallic zigzag nanotubes,  $(3n,0)$ , two squares are plotted for the same diameter  $d_t$ , which explains the split values of the DOS. In contrast, for semiconducting zigzag nanotubes the upper bound and the lower bound of the width  $\Delta E_{11}^S(d_t)$  are determined for two different nanotubes, namely the  $(3n+1,0)$  and  $(3n-1,0)$  nanotubes, respectively, thus explaining the widths  $\Delta E_{ii}^S(d_t)$  in the absence of any splitting of  $E_{ii}^S(d_t)$  by the trigonal warping effect. It is clear from Fig. 6 that at a fixed diameter  $d_t$ , the widths, not only of the  $E_{ii}^M(d_t)$  transitions for the metallic nanotubes, but also of the  $E_{ii}^S(d_t)$  transitions for the semiconducting nanotubes, are determined by the  $E_{ii}(d_t)$  for the zigzag nanotubes. It is noted here that the peak position of the  $E_{ii}^M(d_t)$  for the armchair nanotube is almost at the center of the width delineated by the zigzag nanotubes.

In principle, STM/STS experiments can measure the diameter and chiral angle of an individual carbon nanotube (using STM) and the 1D density of electronic states (using STS) for the nanotube. Therefore, the STM/STS experiments should give individual points in Fig. 7. Such data taken on an ensemble of nanotubes would then yield the ensemble of points in the plot of Fig. 7, thereby clearly showing the dependence of the splitting of the  $E_{ii}(d_t)$  band on the nanotube diameter and chirality.

It is further pointed out that the interband transition energies between vHs, plotted as  $E_{ii}(d_t)$  in Fig. 7, always have a point at  $2\gamma_0/(1-s^2)$  for any nanotube, which corresponds to the vHs peaks which originate from the logarithmic singularity of 2D graphite. This logarithmic singularity comes from the  $M-M$  equi-energy lines in the hexagonal Brillouin zone whose energies are  $\gamma_0/(1-s)$  and  $-\gamma_0/(1+s)$  for the conduction and valence bands, respectively. When the bold lines of the  $k$  vectors cross the  $M-M$  equi-energy lines, the crossing points correspond to a zero value for  $dE/dk$ , which causes a divergence in the DOS in Eq. (15). These peaks can be seen at 2.9 eV for all the metallic nanotubes in Fig. 4. This crossing point is neither a minimum nor a maximum in the energy dispersion relations, but rather is a point of inflection whose second derivative  $d^2E/dk^2$  is zero. Since these DOS peaks can be observed for any nanotube, a determination of the energy where this structure occurs in the STS experiments should provide a good experimental estimation of  $\gamma_0$  and  $s$ . Furthermore, since the energy position of the peak is the same for all nanotubes, these peaks can be observed in a rope sample with a distribution of diameters and chiralities, when we neglect the curvature effect discussed in the Introduction (Sec. I). It is important to note that in the case of zigzag nanotubes with even index,  $(2n,0)$ , a bold line coincides with the  $M-M$  line which gives a strong divergence of the DOS, which can be seen in the  $(18,0)$  trace in Fig. 4. Since this situation occurs for both metallic and semiconducting nanotubes, STS experiments for zigzag nanotubes are most sensitive for obtaining accurate values of  $\gamma_0$  and  $s$ .

When all  $k$  values within the Brillouin zone are included in the calculation of the energies where the singularities in the 1D density of states occur, it is seen in Fig. 4 that for the armchair nanotubes,  $E_{22}^M(d_t)$  is somewhat less than  $2E_{11}^M(d_t)$ , and that for the zigzag nanotubes,  $E_{22}^S(d_t)$  is also not equal to  $2E_{11}^S(d_t)$ , since  $E_{22}^S(d_t)$  and  $2E_{11}^S(d_t)$  come from different symmetry lines on either the  $\Gamma-K$  or  $\Gamma-M$  lines, which is also seen by the opposite bounds on the widths for  $E_{22}^S(d_t)$  and  $2E_{11}^S(d_t)$  for zigzag nanotubes. This is another important aspect of the trigonal warping effect that needs to be considered.

Kataura *et al.*<sup>6</sup> have previously published a very useful plot of the energy separations  $E_{ii}(d_t)$  as a function of  $d_t$ . Figure 7 is basically a re-plot of the work of Kataura *et al.* but Fig. 7 is plotted for  $\gamma_0=2.9$  eV, which yields much better agreement with resonant Raman measurements.<sup>25</sup> The plot in Fig. 7 covers a range of nanotube diameters  $d_t$  from 0.7 to 3.0 nm. Both Fig. 7 and the Kataura *et al.*<sup>6</sup> plot include all  $(n,m)$  values. The Kataura plot includes nanotube diameters  $d_t$  from 0.7 to 1.8 nm and the calculations are based on a value of  $\gamma_0=2.75$  eV. Both plots include both metallic nanotubes ( $n-m=3q$ ) and semiconducting nanotubes ( $n-m\neq 3q$ ). The plot in Fig. 7 also shows that, for a given  $d_t$  value, the points for  $E_{11}^S(d_t)$  are not precisely at  $2a_{C-C}\gamma_0/d_t$ , but show some deviations about this value. The width of the  $E_{ii}(d_t)$  curves at constant  $d_t$  is seen to increase with increasing energy and with increasing  $i$ , so that  $E_{11}^M(d_t)$  exhibits considerably more width than  $E_{11}^S(d_t)$  for a given  $d_t$ . In Fig. 7 it is seen that the width for a given  $E_{ii}(d_t)$  increases as  $d_t$  decreases. For a given carbon nanotube diameter, the resonant width for metallic carbon nanotubes  $E_{11}^M(d_t)$  is larger than  $E_{11}^S(d_t)$  or  $E_{22}^S(d_t)$  for the semiconducting nanotubes. The physical basis for the width of a given  $E_{11}(d_t)$  curve and the deviation of  $E_{11}^S(d_t)$  from  $2E_{11}^S(d_t)$  is due to trigonal warping effects described above. The results of Fig. 7 have been extensively used in discussing various experiments that are sensitive to  $E_{ii}(d_t)$ .<sup>26</sup>

#### IV. RELEVANT EXPERIMENTAL RESULTS

Four different types of experiments can be used to determine the energy separations  $E_{11}(d_t)$ , as discussed in Sec. IV. One of these utilizes the STS/STM (scanning tunneling spectroscopy and microscopy) techniques, which can at least in principle determine the geometrical structure  $(n,m)$  by STM and the energy separations of the vHs  $E_{11}(d_t)$  by STS on the same nanotube.

##### A. STS/STM results

The STS/STM results of Wildöer *et al.*<sup>1</sup> and Odom *et al.*<sup>2</sup> yield measurements of  $E_{ii}(d_t)$  for specific nanotubes, but in almost all cases the diameter of the specific nanotube that was studied by STS was not accurately known. Both research groups interpreted their results within the linear  $k$  approximation [Eqs. (16) and (17)]. On this basis Wildöer *et al.* obtained values of  $\gamma_0=2.7\pm 0.1$  eV for their semiconducting nanotubes and  $\gamma_0=2.9\pm 0.1$  eV for their metallic nanotubes. This deviation in  $\gamma_0$  should be considered to be within the width of  $E_{11}^M(d_t)$  shown in Fig. 7. Odom *et al.*<sup>2</sup> reported

results for semiconducting nanotubes, yielding a value of  $\gamma_0 = 2.5$  eV, significantly lower than values reported by Wildöer *et al.*<sup>1</sup> and by other techniques discussed below. From an experimental standpoint, the STS/STM experiments can be made more accurate by determining  $E_{ii}(d_t)$  for the specific nanotube for which  $(n, m)$  has also been measured.<sup>27</sup> A determination of  $E_{11}^M(d_t) = 1.57$  eV along these lines was recently provided<sup>4</sup> for a (13,7) nanotube, yielding a very low value for  $\gamma_0 = 2.54$  eV. The STM/STS method for determining  $\gamma_0$  is direct, but no corrections have been made for the perturbation of the nanoprobe electric field on the 1D electron density of states.

Furthermore, although the measurements can be made on isolated carbon nanotubes rather than on nanotubes immersed in nanotube bundles, the nanotubes are normally placed on substrates during the measurement process and the effect of the charge transfer between the nanotube and the substrate is not taken into account. Another source of error in interpreting STS data for  $E_{11}(d_t)$  is associated with the trigonal warping effect discussed in this paper and shown in Fig. 7. If the  $(n, m)$  value of the nanotube were known, the effect of trigonal warping would easily be taken into account. Also the asymmetry of the density of states singularities should be taken into account in determining the energy of  $E_{ii}(d_t)$  from a broadened feature in the actual STS data.

### B. Optical measurements

A second method for determining  $E_{11}(d_t)$  comes from optical spectra, where the measurements are made on ropes of single-wall carbon nanotubes, so that appropriate corrections should be made for intertube interactions in interpreting the experimental data. Optical transmission spectra were taken for single-wall nanotubes synthesized using four different catalysts,<sup>6,14</sup> namely NiY (1.24–1.58 nm), NiCo (1.06–1.45 nm), Ni (1.06–1.45 nm), and RhPd (0.68–1.00 nm). For the NiY catalyst, three large absorption peaks were observed at 0.68, 1.2, and 1.7 eV. Although use of Eqs. (16) and (17) yield a value of  $\gamma_0 = 3.0 \pm 0.2$  eV, corrections for trigonal warping effects are necessary to yield a more accurate value of  $\gamma_0$ . Optical spectra were also reported for nanotubes produced with the NiCo, Ni and RbPd catalysts, but the peak values for the absorption bands were not explicitly quoted.<sup>6,14,28</sup> In interpreting the optical transmission data, corrections for the nonlinear  $k$  dependence of  $E(k)$  away from the  $K$  point need to be considered. Once again, asymmetry of the 1D electronic density of states singularities should be taken into account in extracting the  $E_{ii}(d_t)$  from the line shape. Furthermore, the diameter distributions of the nanotubes as well as the difference in gap energies for nanotubes of different chiralities for a given  $d_t$  should be considered in the detailed interpretation of the optical transmission data to yield a value for  $\gamma_0$ . The calculations given in Fig. 7 provide a firm basis for a more detailed analysis.

### C. Resonant Raman scattering experiments

The third determination for single-wall carbon nanotubes (SWNT's) discussed here relates to the analysis of the tangential phonon modes,<sup>8,10,11,25,26,29,30</sup> which can be sensitively probed by resonant Raman spectroscopy. This tech-

nique provides two independent determinations of  $\gamma_0$ , one involving the Stokes spectra (phonon emission), the other involving anti-Stokes spectra (phonon absorption) for the tangential phonon bands. Thus far, almost all of the resonant Raman experiments have been carried out on the Stokes spectra.

In the resonant Raman effect, a large scattering intensity is observed when either the incident or the scattered light is in resonance with electronic transitions between vHs in the valence and conduction bands  $E_{ii}(d_t)$  for a given nanotube  $(n, m)$ . In general, the size of the optical excitation beam is at least 1  $\mu\text{m}$  in diameter, so that many nanotubes with a large variety of  $(n, m)$  values can be excited simultaneously, as is also the case for the optical absorption measurements discussed above. However, the tangential Raman band (between  $\sim 1500$ – $1630$   $\text{cm}^{-1}$ ) associated with the metallic nanotubes is distinctly different from that for semiconducting nanotubes, and this distinction in spectra can be used to establish the width of the metallic window where metallic nanotubes contribute to the resonant Raman spectra.<sup>10,11</sup> Furthermore, from measurement of the radial breathing mode frequency  $\omega_{\text{RBM}}$  in the first-order Raman spectra, the nanotube diameter can be estimated from the diameter  $d_t$  dependence of  $\omega_{\text{RBM}} \propto 1/d_t$ , once the proportionality between  $\omega_{\text{RBM}}$  and one  $(n, m)$  nanotube is established, such as the (10,10) nanotube. Information on the nanotube diameter distribution is available either by transmission electron microscopy (TEM) or from measurement of  $\omega_{\text{RBM}}$  for many laser excitation energies  $E_{\text{laser}}$ . Since it is unlikely that any information on the nanotube chirality distribution is available experimentally, the assumption of equal *a priori* probability can be assumed so that at a given diameter  $d_t$  the resonant Raman effect is sensitive to the width of the  $E_{ii}(d_t)$  plot in Fig. 7. The metallic window is determined experimentally as the range of  $E_{\text{laser}}$  over which the characteristic Raman spectrum for metallic nanotubes is seen, for which the most intense Lorentzian component is at  $1540$   $\text{cm}^{-1}$ . Since there is essentially no Raman scattering intensity for semiconducting nanotubes at this phonon frequency, the intensity  $I_{1540}$  provides a convenient measure for the metallic window. The normalized intensity of the dominant Lorentzian component for metallic nanotubes  $\tilde{I}_{1540}$  (normalized to a reference line) has a dependence on  $E_{\text{laser}}$  given by

$$\tilde{I}_{1540}(d_0) = \sum_{d_t} A \exp\left[\frac{-(d_t - d_0)^2}{\Delta d_t^2/4}\right] [(E_{11}^M(d_t) - E_{\text{laser}})^2 + \gamma_e^2/4]^{-1} [(E_{11}^M(d_t) - E_{\text{laser}} \pm E_{\text{phonon}})^2 + \gamma_e^2/4]^{-1}, \quad (20)$$

where  $d_0$  and  $\Delta d_t$  are, respectively, the mean diameter and the width of the Gaussian distribution of nanotube diameters within the SWNT sample,  $E_{\text{phonon}}$  is the average energy (0.197 eV) of the tangential phonons and the  $+$  ( $-$ ) sign in Eq. (20) refer to the Stokes (anti-Stokes) process,  $\gamma_e$  is a damping factor that is introduced to avoid a divergence of the resonant denominator, and the sum in Eq. (20) is carried out over the diameter distribution. Equation (20) indicates that the normalized intensity  $\tilde{I}_{1540}(d_0)$  for the Stokes process is large when either the incident laser energy is equal to

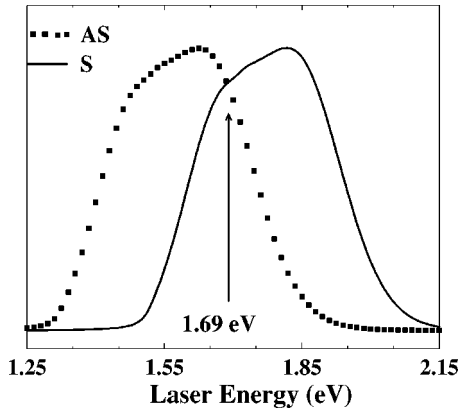


FIG. 8. Metallic window for carbon nanotubes with diameter of  $d_t=1.35$  nm for the Stokes (solid line) and anti-Stokes (square points) processes plotted in terms of the normalized intensity of the Lorentzian phonon component at  $1540\text{ cm}^{-1}$  for metallic nanotubes vs the laser excitation energy for the Stokes and the anti-Stokes scattering processes (Ref. 33). The crossing between the Stokes and anti-Stokes curves is denoted by the vertical arrow.

$E_{11}^M(d_t)$  or when the scattered laser energy is equal to  $E_{11}^M(d_t)$  and likewise for the anti-Stokes process. Since the phonon energy is on the same order of magnitude as the width of the metallic window for nanotubes with  $d_t \sim 1.4$  nm, the Stokes and the anti-Stokes processes can be observed at different resonant energies in the Resonant Raman experiment. The dependence of the normalized intensity  $\tilde{I}_{1540}(d_0)$  for the actual SWNT sample on  $E_{\text{laser}}$  is primarily sensitive<sup>10,11</sup> to the energy difference  $E_{11}^M(d_t)$  for the various  $d_t$  values in the sample, and the resulting normalized intensity  $\tilde{I}_{1540}(d_0)$  is obtained by summing over  $d_t$ , which is conveniently expressed in terms of the average diameter  $d_0$  in  $\tilde{I}_{1540}(d_0)$ .

In Fig. 8 we present a plot of the expected integrated intensities  $\tilde{I}_{1540}(d_0)$  for the resonant Raman process for metallic nanotubes for both the Stokes (solid curve) and anti-Stokes (square points) processes. The figure distinguishes 4 regimes: (1) the semiconducting regime, for which both the Stokes and anti-Stokes spectra receive contributions from semiconducting nanotubes, (2) the metallic regime, where metallic nanotubes contribute to both the Stokes and anti-Stokes spectra, (3) the regime where metallic nanotubes contribute to the Stokes spectra and not to the anti-Stokes spectra, and (4) when the metallic nanotubes contribute only to the anti-Stokes spectra and not to the Stokes spectra. The plot in Fig. 8 is for a nanotube diameter distribution  $d_t = 1.35 \pm 0.20$  nm assuming  $\gamma_e = 0.04$  eV and Eq. (16) was used to calculate the  $E_{11}^M(d_t)$  values. Fits of experimental Raman data to these curves are expected to be very sensitive to the determination of  $\gamma_0$  from the intersection of the Stokes and anti-Stokes curves in Fig. 8, which for the indicated parameters is at 1.69 eV corresponding to  $\gamma_0 = 2.9$  eV.

## V. SUMMARY AND CONCLUSIONS

In summary, the spectra of the DOS for SWNT's have a strong chirality dependence. Especially for the metallic

nanotubes, the DOS peaks are found to be split into two peaks because of the trigonal warping effect, while semiconducting nanotubes do not show a splitting for this reason. The width of the splitting becomes a maximum for the metallic zigzag nanotubes  $(3n,0)$ , and is zero for armchair nanotubes  $(n,n)$ , which are always metallic. In the case of semiconducting nanotubes, the upper and lower bounds of the peak positions of  $E_{11}^S(d_t)$  on the Kataura chart shown in Fig. 7 are determined by the values of  $E_{11}^S(d_t)$  for the  $(3n+1,0)$  or  $(3n-1,0)$  zigzag nanotubes. The upper and lower bounds of the widths of the  $E_{ii}^S(d_t)$  curves alternate with increasing  $i$  between the  $(3n+1,0)$  and  $(3n-1,0)$  zigzag nanotubes.

The existence of a splitting of the DOS spectra for metallic nanotubes can be observed by STS/STM experiments. The width of the metallic window can be observed in the resonant Raman experiments, especially through the differences between the analysis for the Stokes and the anti-Stokes spectra. Some magnetic effects should be observable in the resonant Raman spectra and therefore should affect the 1D DOS for the nanotubes, since the magnetic field will break the symmetry between  $K$  and  $K'$  points. The magnetic susceptibility, which has been important for the determination of  $\gamma_0$  for 3D graphite,<sup>31,32</sup> could also provide interesting results regarding a determination of  $E_{ii}(d_t)$  for SWNT's, including the dependence of  $E_{ii}(d_t)$  on  $d_t$ . Furthermore, we can anticipate future experiments on SWNT's, which could illuminate phenomena showing differences in the  $E(k)$  relations for the conduction and valence bands of SWNT's. Such information would be of particular interest for the experimental determination of the overlap integral  $s$  as a function of nanotube diameter. Purification of SWNT's to provide SWNT's with a known diameter and chirality should be given high priority for progressing research on carbon nanotube physics.

The discussion presented in this paper for the experimental determination of  $E_{ii}(d_t)$  depends on assuming  $s=0$ , in order to make direct contact with the tight-binding calculations. If  $s \neq 0$ , then the determination of  $E_{ii}(d_t)$  would depend on the physical experiment that is used, because different experiments emphasize different  $k$  points in the Brillouin zone. The results of this paper suggest that theoretical tight-binding calculations for nanotubes should also be refined to include the effect of  $s \neq 0$ . Higher-order (more distant neighbor) interactions should yield corrections to the lowest order theory discussed here.

## ACKNOWLEDGMENTS

The authors gratefully acknowledge valuable discussions with Dr. P. C. Eklund, Dr. M. Pimenta, and Dr. C. Dekker. R.S. acknowledges a grant from the Ministry of Education Japan (Grant No. 11165216) and the Japan Society for the Promotion of Science for his visit to MIT. The MIT authors acknowledge support under NSF Grant Nos. DMR 98-04734 and INT 98-15744.

- <sup>1</sup>J. W. G. Wildöer, L. C. Venema, A. G. Rinzier, R. E. Smalley, and C. Dekker, *Nature (London)* **391**, 59 (1998).
- <sup>2</sup>T. W. Odom, J. L. Huang, P. Kim, and C. M. Lieber, *Nature (London)* **391**, 62 (1998).
- <sup>3</sup>T. W. Odom, J. L. Huang, P. Kim, M. Ouyang, and C. M. Lieber, *J. Mater. Res.* **13**, 2380 (1998).
- <sup>4</sup>T. W. Odom (private communication).
- <sup>5</sup>H. Ajiki and T. Ando, *Physica B* **201**, 349 (1994).
- <sup>6</sup>H. Kataura, Y. Kumazawa, N. Kojima, Y. Maniwa, I. Umezū, S. Masubuchi, S. Kazama, X. Zhao, Y. Ando, Y. Ohtsuka, S. Suzuki, and Y. Achiba, in *Proceedings of the International Winter School on Electronic Properties of Novel Materials (IWEPM'99)*, edited by H. Kuzmany, M. Mehring, and J. Fink, (American Institute of Physics, Woodbury, NY, 1999).
- <sup>7</sup>S. Kazaoui, N. Minami, R. Jacquemin, H. Kataura, and Y. Achiba, *Phys. Rev. B* **60**, 13 339 (1999).
- <sup>8</sup>A. M. Rao, E. Richter, S. Bandow, B. Chase, P. C. Eklund, K. W. Williams, M. Menon, K. R. Subbaswamy, A. Thess, R. E. Smalley, G. Dresselhaus, and M. S. Dresselhaus, *Science* **275**, 187 (1997).
- <sup>9</sup>A. Kasuya, Y. Sasaki, Y. Saito, K. Tohji, and Y. Nishina, *Phys. Rev. Lett.* **78**, 4434 (1997).
- <sup>10</sup>M. A. Pimenta, A. Marucci, S. D. M. Brown, M. J. Matthews, A. M. Rao, P. C. Eklund, R. E. Smalley, G. Dresselhaus, and M. S. Dresselhaus, *J. Mater. Res.* **13**, 2396 (1998).
- <sup>11</sup>M. A. Pimenta, A. Marucci, S. Emedocles, M. Bawendi, E. B. Hanlon, A. M. Rao, P. C. Eklund, R. E. Smalley, G. Dresselhaus, and M. S. Dresselhaus, *Phys. Rev. B* **58**, R16 016 (1998).
- <sup>12</sup>J. W. Mintmire and C. T. White, *Phys. Rev. Lett.* **81**, 2506 (1998).
- <sup>13</sup>C. T. White and T. N. Todorov, *Nature (London)* **393**, 240 (1998).
- <sup>14</sup>H. Kataura, Y. Kumazawa, Y. Maniwa, I. Umezū, S. Suzuki, Y. Ohtsuka, and Y. Achiba, *Synth. Met.* **103**, 2555 (1999).
- <sup>15</sup>S. J. Tans, R. M. Verschueren, and C. Dekker, *Nature (London)* **393**, 49 (1998).
- <sup>16</sup>P. Lambin (private communication).
- <sup>17</sup>R. Saito, G. Dresselhaus, and M. S. Dresselhaus, *Physical Properties of Carbon Nanotubes* (Imperial College Press, London, 1998).
- <sup>18</sup>R. Saito, M. Fujita, G. Dresselhaus, and M. S. Dresselhaus, *Phys. Rev. B* **46**, 1804 (1992).
- <sup>19</sup>Ph. Lambin and V. Meunier, in *Proceedings of the Winter School on Electronic Properties Novel Materials*, edited by H. Kuzmany, J. Fink, M. Mehring, and S. Roth, AIP Conf. Proc. **442** (Kirchberg Winter School, Woodbury, NY, 1998), p. 504.
- <sup>20</sup>P. R. Wallace, *Phys. Rev.* **71**, 622 (1947).
- <sup>21</sup>J. W. McClure, *Phys. Rev.* **104**, 666 (1956).
- <sup>22</sup>G. S. Painter and D. E. Ellis, *Phys. Rev. B* **1**, 4747 (1970).
- <sup>23</sup>M. S. Dresselhaus, G. Dresselhaus, K. Sugihara, I. L. Spain, and H. A. Goldberg, *Graphite Fibers and Filaments*, Vol. 5 of *Springer Series in Materials Science* (Springer-Verlag, Berlin, 1988).
- <sup>24</sup>R. A. Jishi, D. Inomata, K. Nakao, M. S. Dresselhaus, and G. Dresselhaus, *J. Phys. Soc. Jpn.* **63**, 2252 (1994).
- <sup>25</sup>G. Dresselhaus, M. A. Pimenta, R. Saito, J. C. Charlier, S. D. M. Brown, P. Corio, A. Marucci, and M. S. Dresselhaus, in *Science and Applications of Nanotubes*, edited by D. Tománek and R. J. Enbody (Kluwer Academic, New York, 2000); *Proceedings of the International Workshop on the Science and Applications of Nanotubes* (Michigan State University, East Lansing, MI, 1999).
- <sup>26</sup>M. S. Dresselhaus, M. A. Pimenta, K. Kneipp, S. D. M. Brown, P. Corio, A. Marucci, and G. Dresselhaus, in *Science and Applications of Nanotubes*, edited by D. Tománek and R. J. Enbody (Kluwer Academic, New York, 2000); *Proceedings of the International Workshop on the Science and Applications of Nanotubes* (Michigan State University, East Lansing, MI, 1999).
- <sup>27</sup>C. H. Olk and J. P. Heremans, *J. Mater. Res.* **9**, 259 (1994).
- <sup>28</sup>H. Kataura (private communication).
- <sup>29</sup>A. Kasuya, M. Sugano, Y. Sasaki, T. Maeda, Y. Saito, K. Tohji, H. Takahashi, Y. Sasaki, M. Fukushima, Y. Nishina, and C. Horie, *Phys. Rev. B* **57**, 4999 (1998).
- <sup>30</sup>M. Sugano, A. Kasuya, K. Tohji, Y. Saito, and Y. Nishina, *Chem. Phys. Lett.* **292**, 575 (1998).
- <sup>31</sup>J. W. McClure, *Phys. Rev.* **108**, 612 (1957).
- <sup>32</sup>K. S. Krishnan, *Nature (London)* **133**, 174 (1934).
- <sup>33</sup>S. D. M. Brown, P. Corio, A. Marucci, M. S. Dresselhaus, M. A. Pimenta, and K. Kneipp, *Phys. Rev. B* (to be published).